J Mater Sci: Mater Electron (2015) 26:1413–1418
DOI 10.1007/s10854-014-2555-1

Thermally stable $BaTiO_3$–$Bi(Zn_{0.75}W_{0.25})O_3$ solid solution with high relative permittivity and low dielectric loss

Xiuli Chen · Jie Chen · Dandan Ma · Huanfu Zhou · Liang Fang

Received: 18 September 2014 / Accepted: 25 November 2014 / Published online: 4 December 2014

Abstract $(1 - x)BaTiO_3$–$xBi(Zn_{0.75}W_{0.25})O_3$ [BT–BZW, $0 \leq x \leq 0.2$] solid solutions were fabricated via a conventional solid-state reaction method. The relationships among compositions, crystal structures, and dielectric properties were investigated. X-ray diffraction patterns showed that a phase transformation from tetragonal to pseudocubic was observed at $0.03 \leq x \leq 0.1$. Raman spectra analysis also illustrated that the long-range ferroelectric order is disrupted from these compositions. Dielectric data showed that as the BZW addition was small ($0.01 \leq x \leq 0.04$), the magnitude of permittivity maxima decreased, and the Curie temperature was almost irrespective of BZW content (x). While the dielectric temperature stability and relative permittivity of BT below the Curie temperature were effectively improved. In particular, the ceramic with $x = 0.04$ possesses the dielectric properties with high permittivity ($\sim$3,000), low dielectric loss (<3 %) and dielectric temperature stability ($\pm$15 %) in the temperature range of 25–125 °C, indicating this ceramic satisfies the requirement of EIA X7R specifications. Especially for $x = 0.2$, the variations of $\Delta\varepsilon/\varepsilon_{100\ ^\circ C}$ is around $\pm$15 % over a wide temperature range from 100 to 400 °C, suggesting potential usage at elevated temperatures.

X. Chen · J. Chen · D. Ma · H. Zhou (✉) · L. Fang
Ministry-Province Jointly-Constructed Cultivation Base for State Key Laboratory of Processing for Non-ferrous Metal and Featured Materials, Guangxi Zhuang Autonomous Region, Key Laboratory of New Processing Technology for Nonferrous Metals and Materials, Ministry of Education, School of Materials Science and Engineering, Guilin University of Technology, Guilin 541004, China
e-mail: zhf_032@163.com

X. Chen
e-mail: cxlnwpu@163.com

1 Introduction

Multilayer ceramic capacitors (MLCCs) are particularly crucial electronic components due to the great demand in transducers, infrared detectors, and pulse generating devices [1, 2]. With the development of electronic devices toward miniaturization and multi-functionality, large dielectric permittivity and relatively low permittivity variation have been imminently required for high performance MLCCs [3]. Most capacitors in microelectronics with excellent electric properties are lead-based perovskite materials, such as Pb(Mg, Nb)O_3, Pb(Zr,Ti)O_3, Pb(Sc,Ta)O_3, etc. [4–12]. Nevertheless, this is at the expense of the environment and human health. Therefore, developing lead-free ferroelectric ceramics is indispensable for environmental protection and human health. As well known, the chemistry of Pb plays an important role in achieving the properties of Pb-based ferroelectrics ceramics [13, 14]. Bi^{3+} is an excellent candidate for the substitution of Pb^{2+} on account of a similar electronic structure [15]. Unfortunately, pure Bi-based perovskite ferroelectric ceramics are difficult to prepare using general sintering method owing to low perovskite tolerance factor (t) [16].

To stabilize Bi-based perovskite structure, some lead-free end members with relatively high perovskite tolerance factor were selected to obtain new compounds, such as $(Bi_{0.5}Na_{0.5})TiO_3$, $K_{0.5}Na_{0.5}NbO_3$, and $BaTiO_3$-based ceramics, etc. [17–21]. $BaTiO_3$ (BT, $t = 1.011$) has been extensively studied for many years owing to its marvelous dielectric properties [22]. Recently, numerous researches on the modification of BT with Bi-based perovskite compounds have been studied, such as BT–$Bi(Zn_{0.5}Ti_{0.5})O_3$, BT-$(Mg_{0.5}Ti_{0.5})O_3$, BT-$(Ni_{0.5}Ti_{0.5})O_3$, and BT-$(Zn_{0.5}Zr_{0.5})O_3$ etc. [22–28]. These solid solutions exhibit excellent temperature-stable dielectric behavior, which is extremely attractive for MLCC application. In our previous study, $(1 - x)BaTiO_3$–$xBi(Mg_{0.75}W_{0.25})O_3$

ceramics exhibited a temperature-insensitive relative high permittivity [29]. Mg^{2+} and Zn^{2+} possess the same valence and close ionic radius. In Pb-based ferroelectric ceramics, xPbTiO$_3$–$(1-x)$Bi$(Zn_{0.75}W_{0.25})O_3$ (PT–BZW) exhibits a good piezoelectric property [30]. Therefore, we could prospect that BaTiO$_3$–Bi$(Zn_{0.75}W_{0.25})O_3$ ceramics can also show outstanding dielectric properties. The objective of this work is to enhance the temperature stability of BaTiO$_3$ ceramic via adding a secondary end member Bi$(Zn_{0.75}W_{0.25})O_3$ and provide promising candidate materials for MLCC application.

2 Experimental

$(1-x)$BT–xBZW $(0 \le x \le 0.2)$ ceramics were prepared by a two-step solid-state reaction method. Starting materials are $BaCO_3$ (≥99 % Guo-Yao Co. Ltd., Shanghai, China), Bi_2O_3 (≥99 % Guo-Yao Co. Ltd., Shanghai, China), TiO_2 (≥99.99 % Guo-Yao Co. Ltd., Shanghai, China), ZnO (≥99 % Guo-Yao Co. Ltd., Shanghai, China), and WO_3 (≥99 % Guo-Yao Co. Ltd., Shanghai, China). Stoichiometric proportions of BT and BZW were mixed in alcohol using zirconia balls for 10 h. The mixtures were dried and calcined at 1,100 and 800 °C for 4 h, respectively. Subsequently, the calcined powders were weighted according to $(1-x)BaTiO_3$–xBi$(Zn_{0.75}W_{0.25})O_3$ [$(1-x)$BT–xBZW, $0 \le x \le 0.2$] and milled for 4 h in the same way as the raw powders. The resultant powders were mixed with 5 wt% of polyvinyl alcohol and pressed into pellets with 12 mm in diameter and 2 mm in thickness by uniaxial pressing at 200 MPa. The pellets were then embedded with calcined powders of the same composition to minimize alkaline elements volatilization and sintered at different temperatures, depending on the adding content of BZW, ranging from 1,250 to 1,410 °C for 2 h in air.

X-ray diffraction (XRD) patterns were recorded at room temperature using an X-ray diffractometer (X'Pert PRO) with CuKα radiation ($\lambda = 0.15406$ nm). The phase analysis for the XRD data was performed with a PanAlytical software (X'Pert High score Plus). Raman spectroscopy was carried out on a Thermo Fisher Scientific DXR using a 6 mW laser with a wavelength of 532 nm. Silver electrodes were coated on both sides of the pellets, and then fired at 650 °C for 30 min. Dielectric properties were measured with an applied voltage of 500 mV over 100 Hz–1 MHz from room temperature to 600 °C using a precision impedance analyzer (Model 4294A, Hewlett-Packard Co., Palo Alto, CA, USA) at a heating rate of 3 °C/min.

3 Results and discussion

Figure 1a shows the XRD patterns of $(1-x)$BT–xBZW ceramics $(0 \le x \le 0.2)$ sintered at their optimized temperatures. Diffraction data confirmed that no trace of secondary peak was detected, which suggests that BZW has diffused into the BT lattices to form a homogenous solid solution. The enlarged XRD patterns in the range of 2θ from 44° to 46° are shown in Fig. 1b. With increasing BZW content, the intensities of $(200)_T$ and $(002)_T$ peaks at around 45° decrease, while the integrated intensities of $(200)_{P-C}$ peak increase remarkably. The samples with composition of $x \le 0.02$ display an obvious splitting of (002)/(200) diffraction peaks in accordance with the tetragonal symmetry (P4 mm) [31]. The pseudo-cubic phase can be obtained for these samples of $x \ge 0.12$ with the merging of $(002)_T$ and $(200)_T$ peaks into a single $(200)_{P-C}$ peak. When $0.03 \le x \le 0.1$, the ceramics show coexistence of tetragonal and pseudocubic phases.

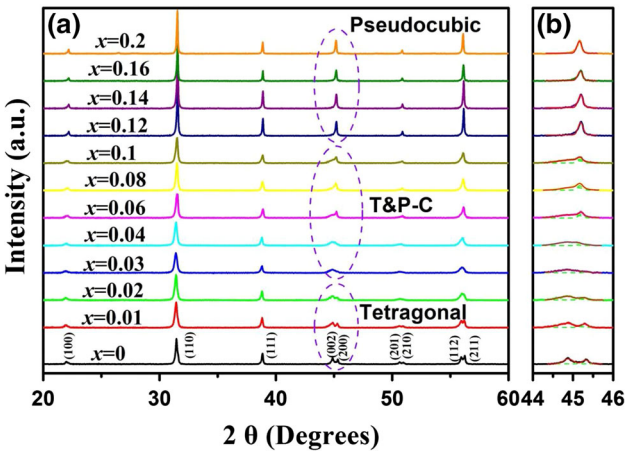

Fig. 1 **a** X-ray diffraction patterns of $(1-x)$BT–xBZW ceramics sintered at their optimized temperatures, and **b** the (002)/(200) diffraction patterns of the sample fitted by Gaussian function in the range 44°–46°

In order to give a better illustration of phase evolution, we carried out the Raman spectra for $(1-x)$BT–xBZW

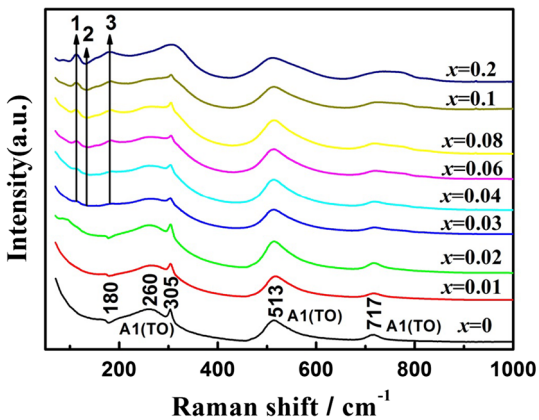

Fig. 2 Room temperature Raman spectra of $(1-x)$BT–xBZW $(0 \le x \le 0.2)$ ceramics in the frequency range of 0–1,000 cm^{-1}

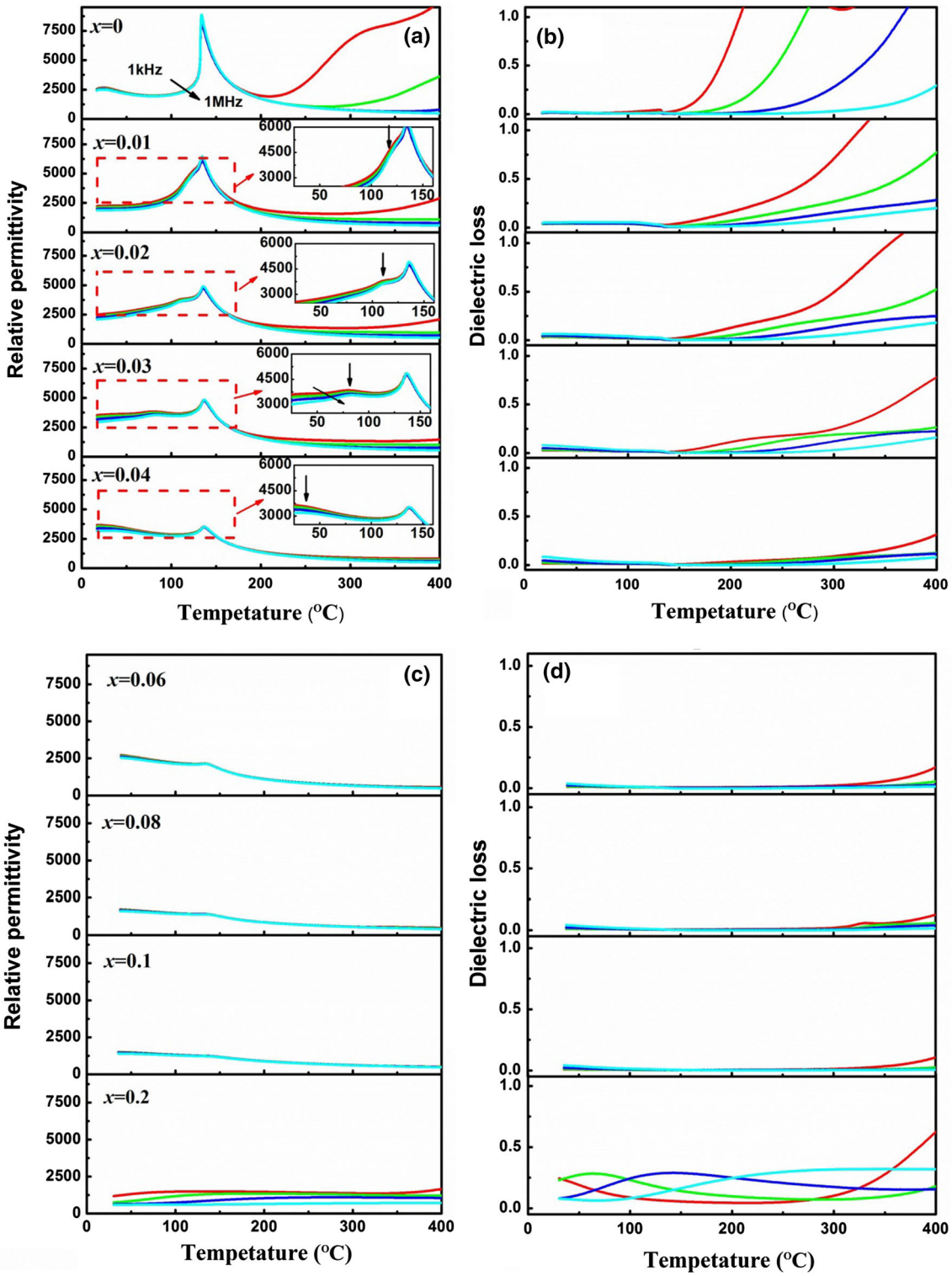

Fig. 3 **a** Temperature dependence of relative permittivity and **b** dielectric loss for $(1 - x)$BT–xBZW ($0 \leq x \leq 0.2$) ceramics measured at 1, 10, 100 kHz and 1 MHz

($0 \leq x \leq 0.2$) ceramics at room-temperature in the frequency range of 0–1,000 cm^{-1}, as shown in Fig. 2. The Raman spectrum of pure $BaTiO_3$ was characterized, by an interference dip at $\sim$180 cm^{-1} and a "silent" mode at $\sim$305 cm^{-1}, which appears only in presence of a long-range ferroelectric phase [32, 33]. It is observed that the sharp E(TO) "silent" mode at 305 cm^{-1} and the resonance dip at 180 cm^{-1} are presented only in tetragonal phases at

$0 \leq x \leq 0.02$. The vanishment of resonance dip at 180 cm^{-1} and the existence of sharp E(TO) "silent" mode at 305 cm^{-1} indicated that the coexistence of tetragonal and pseudocubic phases at $0.03 \leq x \leq 0.1$. For $x = 0.2$, the characteristic of long-range ferroelectric ordering in $BaTiO_3$ is absent in pseudocubic phases. These results agree well with the structural evaluation of XRD patterns, as seen in Fig. 1. In addition, the spectral signature changes dramatically with increasing B-site substituent content ($0.03 \leq x \leq 0.2$), namely the modes 2 appears, a new interference dip 1 is present at $\sim$125 cm^{-1}, which results from the interaction between differently sized octahedra in the lattice [34]. The one at 180 cm^{-1} disappears and in its place a new mode 3 can be observed. The relative intensity of mode 3 also increases with increasing x, as well as the interference dip 2. Modes 1 and 3 are related with A–O vibrations and their appearance suggests that there exists Ba^{2+} or Bi^{3+} cations enriched nano-sized areas (clusters) [35]. Similar spectral signatures associated with local cationic order have been already detected in $BiAlO_3$-modified BT [36].

Figure 3 shows the temperature dependences of relative permittivity and dielectric loss of the $(1 - x)$BT–xBZW ceramics ($0 \leq x \leq 0.2$) from room temperature to 400 °C at 1, 10, 100 kHz, and 1 MHz. Due to the ferroelectric domain dynamics, two characteristic dielectric peaks were observed for $0.01 \leq x \leq 0.04$, corresponding to the ferroelectric–ferroelectric (T_{FE}) and ferroelectric–paraelectric phase transition (T_C), which maybe associate with the particular structure of the grain, as seen in the insert of Fig. 3a. When the BZW addition is small ($0.01 \leq x \leq 0.04$), the first characteristic dielectric peak shifts toward a lower temperature with increasing x and T_C is almost independent on the BZW content. Whereas, with further increasing BZW content ($0.06 \leq x \leq 0.2$), the first characteristic dielectric peak could not be observed above 30 °C. And the T_C was also shifted to lower temperature with $x = 0.1$. The differences in the valence of BT and BZW on the A/B cations (Ba^{2+}, Bi^{3+})/(Zn^{2+}, Ti^{4+}, W^{6+}) usually depress the T_c. The previous researches have reported that the valence mismatch evokes the rapid decrease of T_c [37, 38]. The similar phenomena were found in the $BaTiO_3$–BZZ, BT–BZT and $BiScO_3$–$BaTiO_3$ systems [28, 39, 40]. For $x = 0.2$, the dielectric behavior is strongly dispersive which the relative permittivity decreases and the dielectric loss tangent increases with increasing frequency, displaying a broad plateau-like maximum over a large temperature range, analogous to the dielectric properties of glassy relaxor dielectrics [41–43].

Figure 4a shows the temperature dependences of relative permittivity of the $(1 - x)$BT–xBZW ceramics at 10 kHz from room temperature to 400 °C. When the BZW addition was small ($0.01 \leq x \leq 0.04$), the magnitude of permittivity maxima decreased, which can be explained by

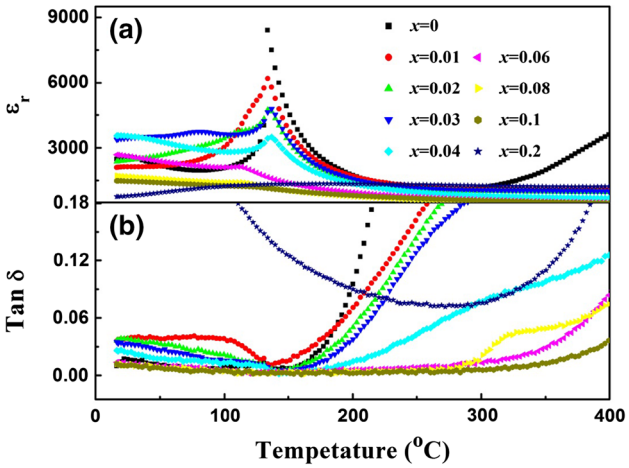

Fig. 4 *a* Temperature dependences of relative permittivity, and *b* dielectric loss of the $(1 - x)$BT–xBZW at 10 kHz from room temperature to 400 °C

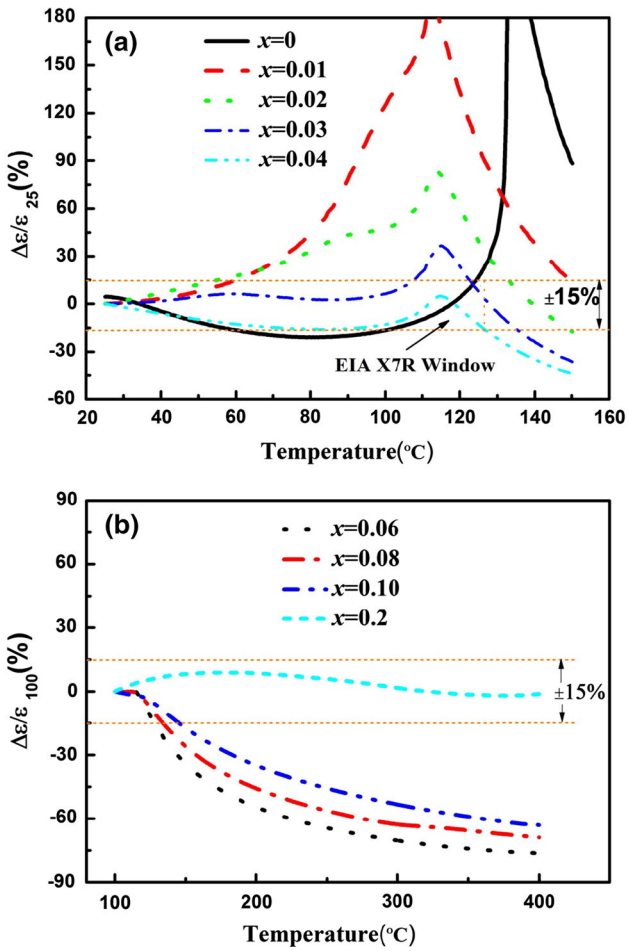

Fig. 5 **a** $\Delta\varepsilon/\varepsilon_{25\ °C}$ as a function of temperature for the $(1 - x)$BT–xBZW ($0 \leq x \leq 0.04$) ceramics at 10 kHz, where $\Delta\varepsilon = \varepsilon_{25\text{–}150\ °C} - \varepsilon_{25\ °C}$ and **b** $\Delta\varepsilon/\varepsilon_{100\ °C}$ as a function of temperature for the $(1 - x)$BT–xBZW ($x = 0.06$, 0.08 0.1, 0.2) ceramics at 10 kHz, where $\Delta\varepsilon = \varepsilon_{100\text{–}400\ °C} - \varepsilon_{100\ °C}$

the suppression in spontaneous polarization and the permittivity maxima, characterizing the ferroelectric transition as increasing the paraelectric phase [44]. While the relative permittivity and dielectric temperature stability below the Curie temperature were effectively improved. Ceramic with relatively stable and high dielectric permittivity (~3,000) was obtained for $x = 0.04$. Meanwhile, the loss tan δ values exhibited a low value ($\leq$0.05) for the compositions of $0 \leq x \leq 0.1$. However, the temperature dependence of tan δ is markedly different above the Curie temperature. Interestingly, for $x = 0.06$, 0.08 and 0.1, tan δ remains relatively low values ($\leq$0.02) up to 300 °C, as shown in Fig. 4b. In contrast, tan δ for $x = 0.2$ has a relatively low value ($\leq$0.18) in a large temperature range from 100 to 400 °C.

Another particular point is the flat temperature coefficient of permittivity. Figure 5 shows $\Delta\varepsilon/\varepsilon_{25\ ^\circ C}$ and $\Delta\varepsilon/\varepsilon_{100\ ^\circ C}$ as a function of temperature for the $(1 - x)$BT–xBZW ($0 \leq x \leq 0.04$) and ($0.06 \leq x \leq 0.2$) ceramics at 10 kHz, respectively. It is clearly seen that the ε–T curves flatten gradually below the Curie temperature with the small BZW addition ($0.01 \leq x \leq 0.04$), as shown in Fig. 5a. Especially, for $x = 0.04$, the ceramic showed a superior dielectric temperature stability (±15 %) with relatively high permittivity (~3,000) and low dielectric loss (<3 %) over the temperature range from room temperature to 125 °C, which satisfies the requirement of the Electronic Industry Association (EIA) X7R type MLCCs [$(\varepsilon - \varepsilon_{RT})/\varepsilon_{RT} \leq \pm$ 15 % in a range of −55 to 125 °C)] [45]. In addition, the variation of $\Delta\varepsilon/\varepsilon_{100\ ^\circ C}$ for $x = 0.2$ is also around ±15 % over the wide temperature range from 100 to 400 °C, as show in Fig. 5b, suggesting a potential usage at elevated temperatures.

4 Conclusions

A combined XRD, Raman and dielectric characterization of $(1 - x)$BT–xBZW ($0 \leq x \leq 0.2$) ceramics have been investigated. XRD analysis suggested that all ceramics were single-phase. A typical tetragonal phase was observed when $x \leq 0.02$ and the coexistence of tetragonal and pseudo-cubic phases appeared at $0.03 \leq x \leq 0.1$ at room temperature. When $x \geq 0.12$, a pseudo-cubic phase can be obtained. Raman spectra for $x = 0.2$ suggested the "ferroelectric" modes are absent. Dielectric data show that with increasing the BZW content ($0.01 \leq x \leq 0.04$), the magnitude of the permittivity maxima decreased, and the Curie temperature are almost independent on the BZW content. While the dielectric temperature stability and the relative permittivity of BT below the Curie temperature can effectively be improved. The ceramic with $x = 0.04$ was found to possess the optimum dielectric performance with relatively high permittivity (~3,000), low dielectric loss (<3 %) and small temperature variation of permittivity (±15 %) in the temperature range of 25–125 °C, indicating a potential application in EIA-X7R specifications. For $x = 0.2$, the variation of $\Delta\varepsilon/\varepsilon_{100\ ^\circ C}$ is around ±15 % over a wide temperature range from 100 to 400 °C, suggesting potential usage at elevated temperatures.

Acknowledgments This work was supported by Natural Science Foundation of China (Nos. 11364012, 51102058, 11464009, and 50962004), Natural Science Foundation of Guangxi (Nos. 2013GXNSFAA019291, 2014GXNSFAA118326, and 2014GXNSFAA118312), Project of Guangxi Scientific Research and Technical Development (No. 1348020-11), Research start-up funds Doctor of Guilin University of Technology (Nos. 002401003281 and 002401003282).

References

1. P.S. Dobal, A. Dixit, R.S. Katiyar, Z. Yu, R. Guo, A.S. Bhalla, J. Appl. Phys. **89**, 8085–8091 (2001)
2. N. Baskaran, A. Ghule, C. Bhongale, R. Murugan, H. Chang, J. Appl. Phys. **91**, 10038–10043 (2002)
3. T.A. Jain, K.Z. Fung, S. Hsiao, J. Chan, J. Eur. Ceram. Soc. **30**, 1469–1476 (2010)
4. J. Chen, H.M. Chan, M.P. Harmer, J. Am. Ceram. Soc. **72**, 593 (1989)
5. G.H. Haertling, J. Am. Ceram. Soc. **82**, 797–818 (1999)
6. B.A. Tuttle, D.A. Payne, Ferroelectrics **37**, 603–606 (1981)
7. G. Singh, V.S. Tiwari, J. Alloys Compd. **523**, 30–35 (2012)
8. L.H. Luo, H.B. Chen, Y.J. Zhu, W.P. Li, H.S. Luo, Y.P. Zhang, J. Alloys Compd. **509**, 8149–8152 (2011)
9. D. Bochenek, R. Skulski, P. Wawrzała, D. Brzezińska, J. Alloys Compd. **509**, 5356–5363 (2011)
10. S. Wongsaenmai, S. Ananta, R. Yimnirun, J. Alloys Compd. **474**, 241–245 (2009)
11. J.Y. Xu, M. Jin, J. Tong, M.L. Shi, X.J. Wu, B.L. Lu, L.Q. Luo, J. Alloys Compd. **449**, 36–39 (2008)
12. S. Wongsaenmai, X.L. Tan, S. Ananta, R. Yimnirun, J. Alloys Compd. **454**, 331–339 (2008)
13. P. Baettig, C.F. Schelle, R. Lesar, Chem. Mater. **17**, 1376–1380 (2005)
14. B.P. Burton, E. Cockayne, U.V. Waghmare, Phys. Rev. B **72**, 064113 (2005)
15. H.L. Du, W.C. Zhou, F. Luo, J. Am. Ceram. Soc. **91**, 2903–2909 (2008)
16. R.E. Eitel, C.A. Randall, T.R. Shrout, Jpn. J. Appl. Phys. **41**, 5999–6002 (2001)
17. Y.Q. Huang, L.F. Gao, Y. Hu, H.Y. Du, Mater. Electron. **18**, 605–609 (2007)
18. F. He, X.L. Chen, J. Chen, Y.L. Wang, H.F. Zhou, L. Fang, J. Mater. Sci. Mater. Electron. **24**, 4346–4350 (2013)
19. Y.L. Wang, X.L. Chen, H.F. Zhou, L. Fang, L.J. Liu, H. Zhang, J. Mater. Sci. Mater. Electron. **24**, 770 (2013)
20. Y.L. Wang, X.L. Chen, C.X. Su, Y.M. Huang, H.F. Zhou, L. Fang, L.J. Liu, J. Mater. Sci. Mater. Electron. **24**, 2873–2879 (2013)
21. R. Koduri, M. Lopez, J. Mater. Sci. Mater. Electron. **19**, 669–675 (2008)
22. C.C. Huang, D.P. Cann, J. Appl. Phys. **104**, 024117 (2008)
23. S. Mr, D. Pk, Appl. Phys. Lett. **86**, 262905 (2005)
24. B. Xiong, H. Hao, S.J. Zhang, H.X. Liu, M.H. Cao, J. Am. Ceram. Soc. **94**, 3412–3417 (2011)

25. J. Chen, X.L. Tan, W. Jo, J. Rödel, J. Appl. Phys. **106**, 034109 (2009)
26. T. Leist, J. Chen, W. Jo, E. Aulbach, J. Suffner, J. Röde, J. Am. Ceram. Soc. **95**, 711–715 (2012)
27. C. Sm, S. Cj, S. Tr, R. Ca, J. Appl. Phys. **98**, 034108 (2005)
28. Y.L. Wang, X.L. Chen, H.F. Zhou, L. Fang, L.J. Liu, H. Zhang, J. Alloys Compd. **551**, 365–369 (2013)
29. J. Chen, X.L. Chen, F. He, Y.L. Wang, H.F. Zhou, L. Fang, J. Electron. Mater. **43**, 1112–1118 (2014)
30. D.M. Stein, M.R. Suchomel, P.K. Daviesa, Appl. Phys. Lett. **89**, 132907 (2006)
31. K. Suzuki, K. Kijima, J. Mater. Sci. **40**, 1289–1292 (2005)
32. R. Farhi, M. El Marssi, A. Simon, J. Ravez, Eur. Phys. J. B **9**, 599–604 (1999)
33. A. Scalabrin, A.S. Chaves, D.S. Shim, S.P.S. Porto, Phys. Status Solidi. B Basic. **79**, 731–742 (1977)
34. D.Y. Lu, X.Y. Sun, M. Toda, J. Phys. Chem. Solids **68**, 650–664 (2007)
35. J. Kreisel, P. Bouvier, M. Maglione, B. Dkhil, A. Simon, Phys. Rev. B **69**, 092104 (2004)
36. S.Y. Zheng, E. Odendo, L.J. Liu, D.P. Shi, Y.M. Huang et al., J. Appl. Phys. **113**, 094102 (2013)
37. V.A. Isupov, Phys. Status Solidi A **181**, 211 (2000)
38. R.J. Bratton, T.Y. Tien, J. Am. Ceram. Soc. **50**, 90 (1967)
39. L. Wang, J.H. Cho, Y.S. Sung, Ferroelectrics **380**, 177–182 (2009)
40. H. Ogihara, C.A. Randall, S. Trolier-McKinstry, J. Am. Ceram. Soc. **92**, 1719–1724 (2009)
41. N.O. Birge, Y.H. Jeong, S.R. Nagel, S. Bhattacharya, S. Susman, Phys. Rev. B **30**, 2306–2308 (1984)
42. P. He, K. Deguchi, M. Hirokane, E. Nakamura, J. Phys. Soc. Jpn. **59**, 1835–1840 (1990)
43. V. Bobnar, J. Holc, M. Hrovat, M. Kosec, J. Appl. Phys. **101**, 074103 (2007)
44. W. Heywang, Ferroelectrics **49**, 3 (1983)
45. D.Y. Lu, Y. Yue, X.Y. Sun, J. Alloys Compd. **586**, 136–141 (2014)